J|A|C|S ARTICLES

Published on Web 07/16/2009

Structure−Performance Correlations in Vapor Phase Deposited Self-Assembled Nanodielectrics for Organic Field-Effect Transistors

Sara A. DiBenedetto, David L. Frattarelli, Antonio Facchetti,* Mark A. Ratner,* and Tobin J. Marks*

Department of Chemistry and the Materials Research Center, Northwestern University, Evanston, Illinois 60208-3113

Received April 21, 2009; E-mail: a-facchetti@northwestern.edu; ratner@northwestern.edu; t-marks@northwestern.edu

Abstract: Organic field-effect transistor (OFETs) are fabricated using thin, vapor-deposited films of both the gate dielectric (vapor-deposited self-assembled nanodielectric, v-SAND) and the organic semiconductor. The nanoscopic self-assembled gate dielectrics are structurally organized via molecular precursor hydrogen-bonding interactions, followed by planarization with a vapor-deposited inorganic SiO_x film. It is shown here that the metal−insulator−semiconductor (MIS) and OFET device electrical properties are sensitive to the v-SAND molecular dipolar orientation. In addition, alternating (organic/inorganic/organic/...) and nonalternating (1 organic layer + 1 inorganic layer) v-SAND microstructural arrangements are investigated, and the microstructures are correlated with MIS and OFET device characteristics. Films with alternating microstructures have larger capacitances than nonalternating films of the same thickness. However, they also have larger leakage currents, associated with the enhanced polarization of well-ordered dipolar films. For pentacene OFETs, the largest mobilities (~3 $cm^2/(V\ s)$) are associated with the high-capacitance nonalternating microstructure, and the lowest mobilities (~0.5 $cm^2/(V\ s)$) are associated with the alternating microstructure. v-SAND gated ambient-stable, n-type organic semiconductors show the opposite trends, where slightly greater OFET performance is observed with the lower-capacitance gate dielectric. For the p-type and one of the n-type v-SAND-based OFETs, the performance (under vacuum and ambient) is comparable to, or surpasses, that of previously reported devices using conventional SiO_2 as the gate dielectric. More importantly, the devices fabricated here operate at far lower voltages. These results indicate that v-SAND dielectrics are promising for future flexible organic electronics requiring low-temperature, solvent-free deposition conditions.

Introduction

The gate dielectric capacitance per area C_i in a field-effect transistor (FET) can be described as a parallel plate capacitor, where $C_i = \varepsilon_o k/d$ and d = the dielectric thickness, k = dielectric permittivity (also can be written as ε_r for the relative permittivity), and ε_o = the permittivity of vacuum. To achieve large capacitances that enable low organic field-effect transistor (OFET) operating voltages, it is necessary to reduce the thickness and/or increase the film dielectric permittivity.[1−3] Classic dielectric theory relates the molecular polarizability tensor ($\bar{\alpha}$, cm^3) to the bulk dielectric permittivity through the Clausius−Mossotti relationship (eq 1):

$$k = \frac{3 + 2(4\pi N)\bar{\alpha}}{3 - (4\pi N)\bar{\alpha}} \quad (1)$$

where N is the molecular number density (molecules/cm^3).[4,5] In an applied electric field, the molecular polarizability (α) is related to the induced molecular dipole moment (μ_i) by eq 2:[6,7]

$$\mu_i = \alpha E + \frac{1}{2}\beta E^2 + ... \quad (2)$$

where E is the applied electric field and β is the nonlinear hyperpolarizability. In this context, an attractive approach to developing high-permittivity SiO_2 gate dielectric alternatives would be to incorporate molecular precursors with large polarizabilities/induced dipole moments assembled in thin, well-ordered, and dense thin films. Research in the field of nonlinear optics (NLO) is well advanced in the fabrication of highly ordered films composed of high-β chromophores, typically having large dipole moments. For example, film fabrication techniques include spin-coating and electric field poling,[8−10] siloxane-based self-assembly of multilayer films,[11−13] various intercalation techniques,[14−17] and hydrogen-bonding assisted physical vapor deposition (PVD).[18−20] This extensive knowledge base makes NLO chromophores especially attractive to

(1) Veres, J.; Ogier, S.; Lloyd, G. *Chem. Mater.* **2004**, *16*, 4543.
(2) Facchetti, A.; Yoon, M.-H.; Marks, T. J. *Adv. Mater.* **2005**, *17*, 1705.
(3) DiBenedetto, S. A.; Paci, I.; Facchetti, A.; Marks, T. J.; Ratner, M. A. *J. Phys. Chem. B* **2006**, *110*, 22394.
(4) Rohleder, J. W.; Munn, R. W. *Magnetism and Optics of Molecular Crystals*; Wiley: New York, 1992.
(5) Ashcroft, N. W.; Mermin, N. D. *Solid State Physics*; Holt, Rinehart, Winston: New York, 1976.
(6) Atkins, P. *Physical Chemistry*; 6th ed.; Freeman: New York, 1998.
(7) Keinan, S.; Ratner, M. A.; Marks, T. J. *Chem. Mater.* **2004**, *16*, 1848.

 10.1021/ja902751e CCC: $40.75

incorporate in gate dielectrics for high-capacitance, low operating voltage OFETs.[21]

In initial studies demonstrating NLO multilayers as FET gate dielectrics, we utilized molecular self-assembled nanodielectrics (SANDs) in which the organic and inorganic organosilane precursors are self-assembled via a layer-by-layer solution-phase growth process to yield the hybrid organic−inorganic multilayers.[23] Since this initial work, there have been other reports of self-assembled monolayer[22] (SAM) and mutilayer[23−25] (SAMT) gate dielectrics affording OFETs with reduced operating voltages[26,27] and/or enhancing performance of complementary circuits compared to the performance with standard thick (100−300 nm) SiO_2 gate dielectrics.[28−30] However, most of these studies rely on solution-based deposition procedures, which can be time-intensive,[20] and the required solvents may be incompatible with some bottom-contact and plastic substrate based FET configurations.[31−33] The PVD approach for film fabrication is promising not only because it is a solvent-free and expeditious process, but it allows precision thickness control in dense film growth.[34−37] Furthermore, designed volatile molecular precursors having appropriate structures ensure control over the propagation of molecular alignment on the substrate surface.[38−40] Recently, in a brief communication, we reported SAND-like films, composed of new NLO building blocks, which are fabricated entirely via vapor-phase processing (v-SAND). In this preliminary study, we found that NLO-based v-SAND materials are effective gate dielectrics for low-voltage, high-mobility pentacene OFETs.[41−46] This contribution goes substantially beyond our communication by discussing in depth the vapor-phase fabrication, microstructural optimization, electrical characterization of the hybrid v-SAND thin films, and structure−performance relationships in the resulting OFETs.

For OFET applications, it is known that current leakage through the gate insulator,[47−49] in addition to the dielectric surface roughness,[50,51] surface energy mismatch,[52−54] and dielectric permittivity,[55−57] can have significant consequences for OFET performance.[58] To this end, the implementation of designed nanoscopic hybrid gate dielectrics is promising since the π-conjugated organic building blocks could potentially provide very large permittivities/capacitances[4] (but also potentially larger leakage currents due to molecular wire/rectifying behavior[59,60]), and the amorphous SiO_x inorganic layer should act as a tunneling barrier that helps suppress leakage current.[61−64]

(8) Pereverzev, Y. V.; Gunnerson, K. N.; Prezhdo, O. V.; Sullivan, P. A.; Liao, Y.; Olbricht, B. C.; Akelaitis, J. P.; Jen, A. K.-Y.; Dalton, L. R. *J. Phys. Chem. C* **2008**, *112*, 4355.
(9) Dalton, L. R.; Sullivan, P. A.; Olbricht, B. C.; Takimoto, Y.; Rehr, J. J.; Eichinger, B. E.; Mistry, A. A.; Bale, D.; Rommel, H.; Robinson, B. *Proc. SPIE−Int. Soc. Opt. Eng.* **2007**, *6638*, 663801.
(10) Zhu, P.; van der Boom, M. E.; Kang, H.; Evmenenko, G.; Dutta, P.; Marks, T. J. *Chem. Mater.* **2002**, *14*, 4982.
(11) van der Boom, M. E.; Zhu, P.; Malinsky, J. E.; Lin, W.; Dutta, P.; Marks, T. J. *Langmuir* **2002**, *18*, 3704.
(12) Yitzchaik, S.; Marks, T. J. *Acc. Chem. Res.* **1996**, *29*, 197.
(13) Lin, W.; Lee, T.-L.; Lyman, P. F.; Lee, J.; Bedzyk, M. J.; Marks, T. J. *J. Am. Chem. Soc.* **1997**, *119*, 2205.
(14) Hata, H.; Kubo, S.; Kobayashi, Y.; Mallouk, T. E. *J. Am. Chem. Soc.* **2007**, *129*, 3064.
(15) Ulman, A. *Chem. Rev.* **1996**, *96*, 1533.
(16) Yam, C. M.; Dickie, A. J.; Kakkar, A. K. *Langmuir* **2002**, *18*, 8481.
(17) Park, M. H.; Jang, Y. J.; Sung-Suh, H. M.; Sung, M. M. *Langmuir* **2004**, *20*, 2257.
(18) Altman, M.; Zenkina, O.; Evmenenko, G.; Dutta, P.; van der Boom, M. E. *J. Am. Chem. Soc.* **2008**, *130*, 5040.
(19) Facchetti, A.; Annoni, E.; Beverina, L.; Morone, M.; Zhu, P.; Marks, T. J.; Pagani, G. A. *Nat. Mater.* **2004**, *3*, 910.
(20) Zhu, P.; Kang, H.; Facchetti, A.; Evmenenko, G.; Dutta, P.; Marks, T. J. *J. Am. Chem. Soc.* **2003**, *125*, 11496–11497.
(21) Katz, H. E.; Schilling, M. L. *Chem. Mater.* **1993**, *5*, 1162.
(22) Fontaine, P.; Goguenheim, D.; Deresmes, D.; Vuillaume, D.; Garet, M.; Rondelez, F. *Appl. Phys. Lett.* **1993**, *62*, 2256.
(23) Yoon, M.-H.; Facchetti, A.; Marks, T. J. *Proc. Natl. Acad. Sci. U.S.A.* **2005**, *102*, 4678.
(24) Lee, B. H.; Ryu, M. K.; Choi, S.-Y.; Lee, K.-H.; Im, S.; Sung, M. M. *J. Am. Chem. Soc.* **2007**, *129*, 16034.
(25) Chauhan, A. K.; Aswal, D. K.; Koiry, S. P.; Gupta, S. K.; Yakhmi, J. V.; Surgers, C.; Guerin, D.; Lenfant, S.; Vuillaume, D. *Appl. Phys. A: Mater. Sci. Process.* **2008**, *90*, 581.
(26) Collet, J.; Tharaud, O.; Chapoton, A.; Vuillaume, D. *Appl. Phys. Lett.* **2000**, *76*, 1941.
(27) Halik, M.; Klauk, H.; Zschieschang, U.; Schmid, G.; Dehm, C.; Schutz, M.; Maisch, S.; Effenberger, F.; Brunnbauser, M.; Stellacci, F. *Nature* **2004**, *431*, 963.
(28) Klauk, H.; Zschieschang, U.; Pflaum, J.; Halik, M. *Nature* **2007**, *445*, 745.
(29) Ju, S.; Li, J.; Lui, J.; Chen, P.-C.; Ha, Y.-G.; Ishikawa, F.; Change, H.; Zhou, C.; Facchetti, A.; Janes, D. B.; Marks, T. J. *Nano Lett.* **2008**, *8*, 997.
(30) Smits, E. C. P.; et al. *Nature* **2008**, *455*, 956.
(31) Yan, H.; Zheng, Y.; Blache, R.; Newman, C.; Lu, S.; Woerle, J.; Facchetti, A. *Adv. Mater.* **2008**, *9999*, 1.
(32) Briseno, A.; Mannsfeld, S. C. B.; Ling, M. M.; Liu, S.; Tseng, R. J.; Reese, C.; E., R. M.; Yang, Y.; Wudl, F.; Bao, Z. *Nature* **2006**, *444*, 913.
(33) Jeong, S.; Kim, D.; Moon, J. *J. Phys. Chem. C* **2008**, *112*, 5245.
(34) von Muhlenen, A.; Castellani, M.; Schaer, M.; Zuppiroli, L. *Phys. Status Solidi B* **2008**, *245*, 1170.
(35) Lin, W.; Yitzchaik, S.; Malik, A.; Durbin, A. K.; Richter, A. G.; Wong, G. K.; Dutta, P.; Marks, T. J. *Angew. Chem., Int. Ed. Engl.* **1995**, *34*, 1497.
(36) Roscoe, S. B.; Yitzchaik, S.; Kakkar, A. K.; Marks, T. J.; Xu, Z.; Zhang, T.; Lin, W.; Wong, G. K. *Langmuir* **1996**, *12*, 5338.
(37) Choubey, A.; Kwon, O.-P.; Jazbinsek, M.; Günter, P. *Cryst. Growth Des.* **2007**, *7*, 402.
(38) Morotti, T.; Calabrese, V.; Cavazzini, M.; Danilo, P.; Cozzuol, M.; Licciardello, A.; Tuccitto, N.; Quici, S. *Dalton Trans.* **2008**, *3*, 2974.
(39) Schneider, H.-J. *Angew. Chem., Int. Ed. Engl.* **1991**, *30*, 1417.
(40) Burtman, V.; Zelichenok, A.; Yitzchaik, S. *Angew. Chem., Int. Ed.* **1999**, *38*, 2041.
(41) DiBenedetto, S. A.; Frattarelli, D.; Ratner, M. A.; Marks, T. J. *J. Am. Chem. Soc.* **2008**, *130*, 7528.
(42) Bolink, H. J.; Coronado, E.; Sessolo, M. *Chem. Mater.* **2009**, *21*, 439.
(43) Jiang, Y.; Zhang, L.; Yang, D.; Li, L.; Zhang, Y.; Jiang, Z. *Ind. Eng. Chem. Res.* **2008**, *47*, 2495.
(44) Lee, K.; Lu, G.; Facchetti, A.; Janes, D. B.; Marks, T. J. *Appl. Phys. Lett.* **2008**, *92*, 123509.
(45) DiSalvo, F. J. *Advancing Materials Research*; National Academy Press: Washington, DC, 1987.
(46) Mitzi, D. B. In *Functional Hybrid Materials*, 2004; pp 347−386.
(47) de Boer, B.; Iosad, N. N.; Stassen, A. F.; Klapwijk, T. M.; Morpurgo, A. F. *Appl. Phys. Lett.* **2005**, *86*, 032103.
(48) Wilk, G. D.; Wallace, R. M. *J. Appl. Phys. Rev.* **2001**, *89*, 5243.
(49) Boulas, C.; Davidovits, J. V.; Rondelez, F.; Vuillaume, D. *Phys. Rev. Lett.* **1996**, *76*, 4797.
(50) Dimitrakopoulos, C. D.; Malenfant, P. R. L. *Adv. Mater.* **2002**, *14*, 99.
(51) Kelley, T. W.; Boardman, L. D.; Dunbar, T. D.; Muyres, D. V.; Pellerite, M. J.; Smith, T. P. *J. Phys. Chem. B* **2003**, *107*, 5877.
(52) Yang, S. Y.; Shin, K.; Park, C. E. *Adv. Funct. Mater.* **2005**, *15*, 1806.
(53) Miskiewicz, P.; Kotarba, S.; Jung, J.; Marszalek, T.; Mas-Torrent, M.; Gomar-Nadal, E.; Amabilino, D. B.; Rovira, C.; Veciana, J.; Maniukiewicz, W.; Ulanski, J. *J. Appl. Phys.* **2008**, *104*, 054509.
(54) Fritz, S. E.; Kelly, T. W.; Frisbie, D. *J. Phys. Chem. B* **2005**, *109*, 10574.
(55) Kobayashi, S.; Nishikawa, T.; Takenobu, T.; Mori, S.; Shimoda, T.; Mitani, T.; Shimotani, H.; Yoshimoto, N.; Ogawa, S.; Iwasa, A. *Nat. Mater.* **2004**, *3*, 317.
(56) Stassen, A. F.; de Boer, R. W. I.; Iosad, N. N.; Morpurgo, A. F. *Appl. Phys. Lett.* **2004**, *85*, 3899.
(57) Hulea, I. N.; Fratini, S.; Xie, H.; Mulder, C. L.; Iossad, N. N.; Rastelli, G.; Ciuchi, S.; Morpurgo, A. F. *Nat. Mater.* **2006**, *5*, 982.
(58) Uno, M.; Tominari, Y.; Takeya, J. *Org. Electron.* **2008**, *9*, 753.
(59) McCreery, R. L. *Chem. Mater.* **2004**, *16*, 4477.
(60) Metzger, R. M.; Xu, T.; Peterson, I. R. *J. Phys. Chem. B* **2001**, *105*, 7280.
(61) Depas, M.; Van Meirhaeghe, R. L.; Laflere, W. H.; Cardon, F. *Solid-State Electron.* **1994**, *37*, 433–441.

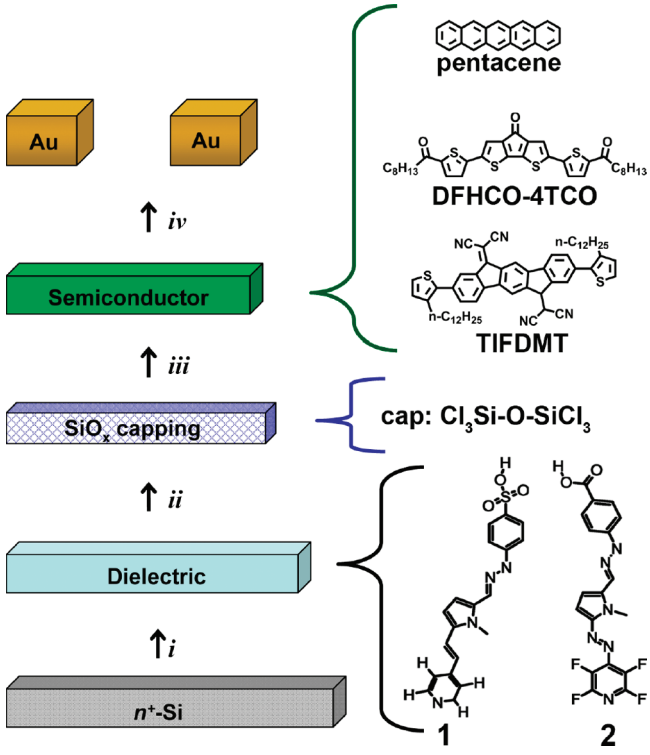

Figure 1. OFET layers and the corresponding chemical structures used for each layer in this study: (i) vapor deposition of **1** or **2**, (ii) exposure of **F1** or **F2** to Cl_6Si_2O vapor, completing the v-SAND structure, (iii) vapor deposition of either pentacene, **DFHCO-4TCO**, or **TIFDMT**, and (iv) vapor deposition of Au source and drain electrodes through a shadow mask to complete the OFET device.

The present contribution explores the vapor-phase deposition of hybrid organic−inorganic nanodielectrics to simultaneously achieve large supramolecular k values, while also maintaining low leakage current through the gate dielectric. First, we investigate the effect of inorganic/organic building block thicknesses on v-SAND-based MIS (metal−insulator−semiconductor) capacitor and OFET device metrics. Next, we capitalize on the planar surface-hydroxylated SiO_x inorganic layers[10,23] to build up alternating organic−inorganic multilayer v-SANDs. It will be seen that by varying the inorganic/organic building block thicknesses and microstructural arrangements, the MIS leakage currents and OFET mobilities can be substantially tuned.[65] Finally, we expand the range of applicable semiconducting materials by demonstrating that two n-type organic semiconductors are also compatible with v-SAND gate dielectrics under both vacuum and ambient measurement conditions.

Experimental Section

See the Supporting Information for more details about materials, methods, and characterization.

Dielectric Film Fabrication. Device fabrication follows the scheme in Figure 1. First, heavily doped n^+-Si substrates were cut from Si(100) wafers using minimal scratches to avoid creating Si particles on the polished surface. The cut substrates were solvent-cleaned by dipping (in two beakers, sequentially, for 30 s each) in pure ethanol (Aldrich, ACS grade, 200 proof) with sonication and were then dried with a filtered stream of nitrogen. Films of **1** or **2** (**F1**, **F2**) were vapor-deposited onto the n^+-Si substrates maintained at room temperature under high vacuum (10^{-6} Torr) using a Denton vacuum (DV-502A) chamber equipped with a diffusion pump (step i, Figure 1). Films were grown at a rate of 0.2 Å/s, and the deposition rate was monitored by an in situ quartz crystal microbalance connected to an Inficon deposition monitor. The thickness of the molecular component (**1** or **2**) could be precisely varied over a range of 3−15 nm to evaluate the dependence of film electrical properties on film thickness.

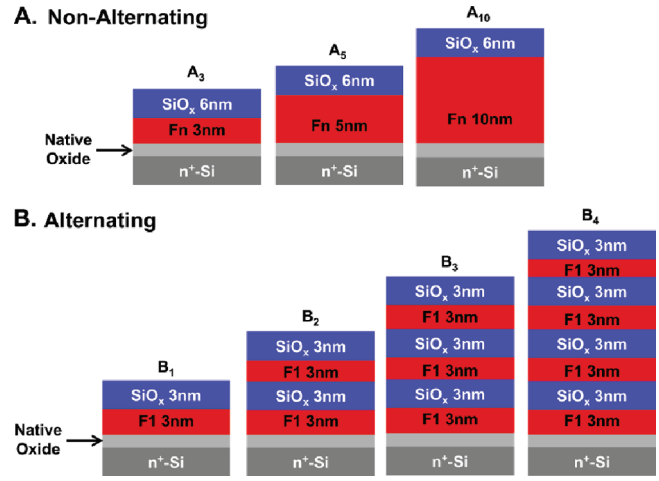

Figure 2. v-SAND nanodielectric microstructures fabricated via the different organic (**1** or **2**) and inorganic precursor deposition sequences: (A) nonalternating microstructure, $\mathbf{A}_x$, where x = thickness of the molecular layer and **Fn** indicates molecular precursor **1** or **2**, and (B) alternating microstructure, $\mathbf{B}_x$, where x = 1, 2, 3, or 4 for the number of repeated (organic−inorganic) bilayers.

Results and Discussion

The SiO_x capping layer thickness is first optimized by investigating MIS device electrical properties versus length of exposure time to the Cl_6Si_2O precursor vapor. The effect of increasing SiO_x thickness on the leakage current and OFET properties is then investigated using two different v-SAND microstructures (Figure 2): (A) nonalternating microstructure where the molecular layer thickness is varied and the **cap** exposure time is held constant. This is called microstructure $\mathbf{A}_x$, where x = the thickness of the organic molecular layer; (B) alternating microstructure having organic and **cap** component layers of constant thickness. Thicker dielectric films are grown by repeated alternating deposition of organic and inorganic layers. This arrangement of components is called $\mathbf{B}_x$, where x = 1, 2, 3, or 4 for the number of (organic−inorganic) repeated bilayers. We first discuss trends in electrical characteristics for the various v-SAND microstructures and molecular building block structures in MIS capacitors, followed by the trends in OFET performance. For this, pentacene and two n-type organic semiconductors are evaluated in v-SAND-based OFETs. The performance characteristics correlate with the gate dielectric capacitance and leakage current, as well as with the dielectric and semiconductor film microstructures.

1. MIS Device Response As a Function of v-SAND Thickness. Thin-film microstructures, thicknesses, and surface morphologies of the vapor-deposited dielectrics were studied by specular X-ray reflectivity[66] (XRR) and tapping mode atomic force microscopy (AFM). Capacitance and leakage current data

(62) Osada, M.; Ebina, Y.; Funakubo, H.; Yokoyama, S.; Kiguchi, T.; Takada, K.; Sasaki, T. *Adv. Mater.* **2006**, *18*, 1023–1027.
(63) Bohr, M. T.; Chau, R. S.; Ghani, T.; Mistry, K. *IEEE Spectum* **2007**, *10*, 29.
(64) Hu, H.; Zhu, C.; Lu, Y. F.; Li, M. F.; Cho, B. J.; Choi, W. K. *IEEE Electron Device Lett.* **2002**, *23*, 514.
(65) Sandberg, H. G. O.; Backlund, T. G.; Osterbacka, R.; Shkunov, M.; Sparrowe, D.; McCulloch, I.; Stubb, H. *Org. Electron.* **2005**, *6*, 142.

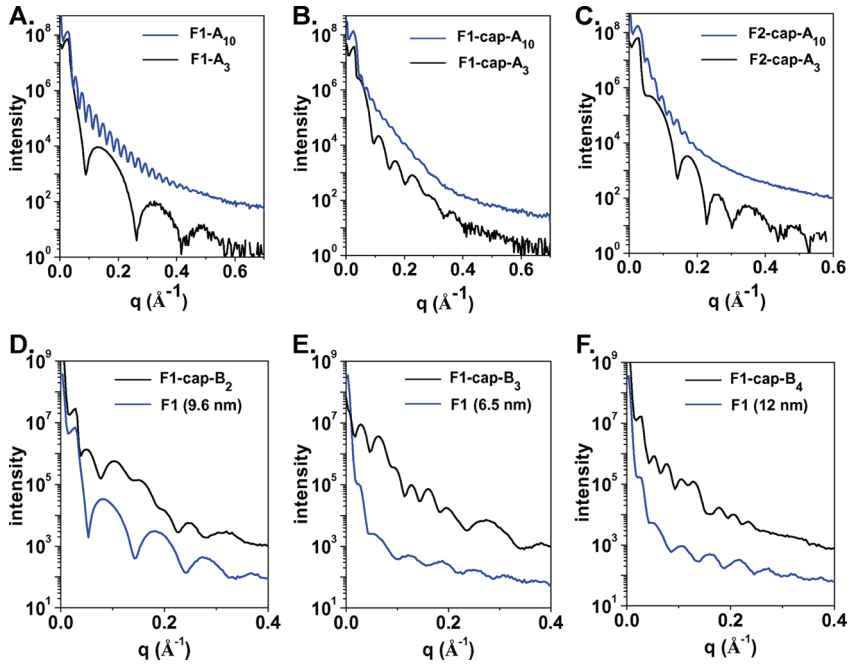

Figure 3. XRR spectra of the indicated v-SAND structures on n^+-Si substrates: (A) **F1**, (B) **F1-cap**, and (C) **F2-cap** having the $\mathbf{A}_x$ type of microstructure. Samples having different organic molecular layer thicknesses are shown, where the black line indicates ~3 nm and the blue line indicates ~10 nm. (D−F) XRR spectra of the indicated v-SAND structures: **F1-cap** in the $\mathbf{B}_x$ microstructure for increasing numbers of organic−inorganic repeat units: (D) $\mathbf{B_2}$, (E) $\mathbf{B_3}$, (F) $\mathbf{B_4}$. The black line indicates alternating **cap** and **F1** microstructure, and the blue line indicates pure **F1**.

for the SiO_x capped (**Fn-cap**) and uncapped (**Fn**) films deposited on Si/native SiO_2 substrates were collected on Si/SiO_2/v-SAND/Au MIS devices. The thicknesses of the molecular layers were varied from "monolayer" to thicker via the vapor deposition process described in the Experimental Section. The sample thicknesses were measured by XRR (vide infra). The AFM images reveal that all of the dielectrics have relatively smooth surfaces with rms roughnesses between 0.35 and 0.50 nm for uncapped films and between 0.6 and 1.8 nm for SiO_x-capped films. Low gate dielectric rms roughness values are known to be important for optimum performance/deposition of the semiconductor in top-contact OFETs.[67] See Supporting Information Figure S1 for representative AFM images of SiO_x capped and uncapped v-SAND films. In the present full study, the thickness is optimized for low leakage currents and high capacitances by varying the length of exposure time of the molecular films to Cl_6Si_2O ($Cl_3SiOSiCl_3$) precursor molecule vapors (Supporting Information Figure S2). A compromise between moderate capacitance and low leakage current is found with a 20 min exposure to the SiO_x precursor vapor, corresponding to an ~6 nm thick SiO_x film, used in the nonalternating v-SAND microstructural arrangement $\mathbf{A_x}$ (Figure 2A). To capitalize on the larger capacitances achieved by using thinner inorganic layers, 3 nm of SiO_x capping was used in the alternating microstructure films $\mathbf{B_x}$ (Figure 2B), where the alternating organic−inorganic layers should, in principle, compensate and suppress current leakage through the thinner **cap** layers.

The film microstructures of the two different v-SAND arrangements are compared quantitatively in the XRR reflectivity spectra of Figure 3.

Both types of microstructural arrangements exhibit a large number of small-angle oscillations/fringes assignable to Kiessig fringes. These indicate a smooth film surface, with more pronounced features indicating ordering at the various substrate−film interfaces.[66,68,69] The overall shape of all of the curves for the $\mathbf{A_x}$ microstructures is similar, and as the total thickness increases, the periodicity of the oscillations decreases, as expected. In principle, a scan from an alternating multilayer sample ($\mathbf{B_x}$ microstructure) should exhibit two types of features: (i) Kiessig fringes,[70] where the minima correspond to the destructive interference of the reflections from the top and bottom of the film and the total film thickness d_{tot} is estimated by $d_{tot} = 2\pi/\Delta k_z$ (Δk_z = spacing between the minima), and (ii) Bragg peaks corresponding to the thickness of the (organic−inorganic) bilayer $d_{bi} = 2n\pi/\Delta k_{ZP}$ (Δk_{ZP} = the position, and n is the order of the Bragg peak). For well-ordered films, $d_{tot} = nd_{bi}$ where n is the number of bilayers.[71] Indeed, there are differences in the oscillation patterns of the spectra in Figure 4D−F. The **F1** samples (blue lines) exhibit one type of oscillation (Kiessig fringes), whereas the $\mathbf{B_x}$ microstructures (black lines) exhibit two major periodicity patterns corresponding to both Kiessig fringes (total film thickness) and Bragg peaks (bilayer thicknesses). The average bilayer thickness estimated from these spectral features is 5.9 nm, consistent with the optimized deposition conditions of the organic and inorganic layers described above. Furthermore, total multilayer thickness (d_{tot}) calculated from the Kiessig fringes matches the d_{tot} calculated from the position of the Bragg peaks (nd_{bi}, see Table 1), indicating consistent periodicity changes perpendicular to

(66) Tolan, M. *X-Ray Scattering from Soft-Mater Thin Films*; Springer: Berlin, 1999.
(67) Stadholder, B.; Hass, U.; Maresch, H.; Haase, A. *Phys. Rev. B* **2006**, *74*, 165302.
(68) Evmenenko, G.; Mo, H.; Kewalramani, S.; Dutta, P. *Langmuir* **2007**, *22*, 6245.
(69) Durr, A. C.; Schreiber, F.; Munch, M.; Karl, N.; Krause, B.; Kruppa, V.; Dosch, H. *Appl. Phys. Lett.* **2002**, *81*, 2276.
(70) Kiessig, H. *Ann. Phys.* **1931**, *10*, 769.
(71) Malik, A.; Lin, W.; Durbin, M. K.; Marks, T. J.; Dutta, P. *J. Chem. Phys.* **1997**, *107*, 645.

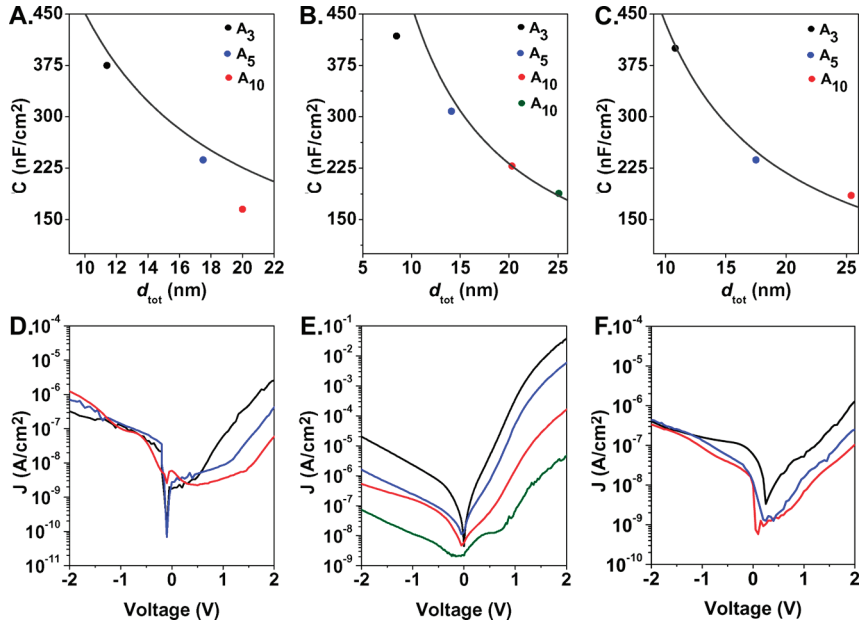

Figure 4. MIS characteristics of v-SAND dielectrics. (A−C) Capacitances measured at 2.0 V are plotted vs XRR-derived thickness of the molecular layer. The different plots are for (A) **F1-cap** in the $\mathbf{A}_x$ microstructure, (B) **F1-cap** in the $\mathbf{B}_x$microstructure, and (C) **F2-cap** in the $\mathbf{A}_x$ microstructure, with the black solid lines showing computed capacitance values. (D−F) Leakage $J-V$ plots, where each curve represents a different thickness as indicated by the legends in panels A−C, for $\mathbf{A}_x$ **F1-cap** (D), $\mathbf{B}_x$ **F1-cap** (E), and $\mathbf{A}_x$ **F2-cap** (F).

Table 1. Comparison of Multilayer Thickness Calculated Using Kiessig Fringes and Bragg Peaks

n (no. of layers)	Kiessig (d_{tot}, nm)	Bragg (nd_{bi}, nm)
1	6.97	
2	12.6	12.5
3	18.8	18.5
4	23.6	23.3

the surface and corresponding to the repeated bilayers. Using this method, the derived uncertainty in thickness is ±5 Å, and the derived uncertainty in the measured periodicity is ±1.25 Å, similar to that reported previously for hydrogen-bonded silane self-assembled multilayers.[72]

The MIS-derived capacitances of the **F1-cap** v-SAND dielectrics in both the $\mathbf{A_x}$ and $\mathbf{B_x}$ microstructures are shown in Figure 4, parts A and B, respectively. The capacitance of **F2-cap** having the $\mathbf{A_x}$ microstructure is shown in Figure 4C for comparison.

The theoretical dielectric constants are derived using Clausius−Mossotti k values of **1** and **2**. For **1**, $\alpha_{zz} = 86.1 \times 10^{-24}$ cm^3, and for **2**, $\alpha_{zz} = 91.1 \times 10^{-24}$ cm^3, corresponding to k's (via eq 1) of 8.8 and 10.7 for **1** and **2**, respectively. These values are next used in the parallel plate capacitor equation (for three capacitors in series: $1/[C_{\text{native oxide}} + C_{\text{molecular}} + C_{\text{capping}}]$) to estimate the v-SAND capacitances based on the computed α_{zz} values. Note that the XRR-derived v-SAND thicknesses were used in the calculations (gray lines in Figure 5A−C), with $d_{no} = 1.5$ nm and $k_{no} = k_{cap} = 3.9$. For each microstructural arrangement of the organic and inorganic layers, the measured capacitance values decrease as the thickness is increased, as expected from the parallel plate capacitor model and indicating reasonable dielectric response. However, the capacitance of the $\mathbf{A_x}$ **F1-cap** series diverges from the parallel plate capacitor calculated values as the thickness increases. In contrast, the

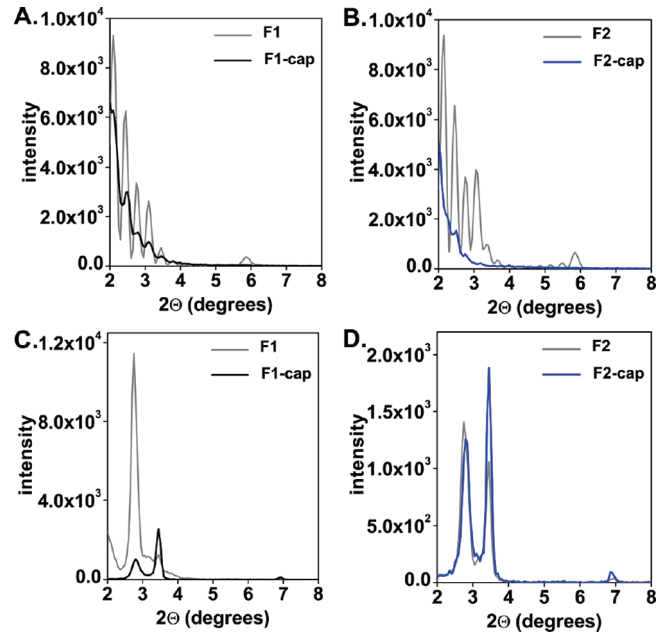

Figure 5. XRD spectra of **DFHCO-4TCO** (A and B) and **TIFDMT** (C and D) films grown on $\mathbf{A_3}$ v-SAND dielectrics **F1-cap** (black) and **F2-cap** (blue). The gray curves in each spectrum correspond to the result for each **Fn** dielectric without SiO_x capping.

trends in the **F2-cap** and the $\mathbf{B_x}$ **F1-cap** v-SANDs track well with calculated values even as the thickness is increased. This can be explained by different molecular hydrogen-bonding interactions operative during film growth, resulting in different molecular dipole orientations (see details in the discussion below).

Although the capacitances of the $\mathbf{B_x}$ films are larger than those of the $\mathbf{A_x}$ films, the leakage currents appear to be adversely affected by the alternating microstructure. For similar $\mathbf{A_x}$ and $\mathbf{B_x}$ film thicknesses, the leakage currents of the $\mathbf{B_x}$ films (Figure 4E) are larger than those of the $\mathbf{A_x}$ films (Figure 4, parts D and

(72) Maoz, R.; Sagiv, J.; Degenhardt, D.; Mohwald, H.; Quint, P. *Supramol. Sci.* **1995**, *2*, 9.

Table 2. Film Thicknesses of **F1-cap** and **F2-cap** (d_{tot}), **F1** and **F2** (d_{uncap}), and SiO_x **cap** ($d_{tot} - d_{uncap} = d_{cap}$) Measured by XRR[a]

	d_{tot} (nm)	d_{uncap} (nm)	d_{cap} (nm)	C_{tot} (nF/cm^2)	k_{molec}	J (A/cm^2)
F1-cap						
A_3	11.4	3.4	6.5	375	11.0	2.6×10^{-6}
A_5	17.5	5.0	11.0	237	9.5	4.2×10^{-6}
A_{10}	20	12.8	5.7	165	3.6	5.9×10^{-8}
F2-cap						
A_3	10.8	3.7	5.6	392	9.4	1.3×10^{-6}
A_5	17.5	4.3	11.7	265	12.3	2.5×10^{-7}
A_{10}	25.4	10.0	13.9	185	12.0	1.0×10^{-7}
F1-cap						
B_1	8.5	3.9	3.0	425	4.0	3.8×10^{-2}
B_2	14	6.5	5.4	307	5.9	5.9×10^{-3}
B_3	20	9.6	9.2	227	8.4	1.6×10^{-4}
B_4	25	12	11	187	7.5	4.4×10^{-6}

[a] MIS-derived capacitances (C_{tot}) at +2.0 V, derived dielectric permittivities (k) based on the measured values of d and C, and leakage currents (J) at +2.0 V. Note that $d_{native\ oxide} = 1.5$ nm is included in d_{tot}.

F). This greater current leakage can be attributed, in part, to the smaller thickness of the SiO_x **cap** layer (3 nm), which is not sufficient to trap polarization-induced leakage current.[73] Furthermore, we suspect that the alternating microstructure affects the dipole orientation/ordering of **1**, resulting in maximum polarization, P ($P = \langle\mu\rangle N$, where $\langle\mu\rangle$ = average dipole moment, and N = number density[6,74]), and current leakage.[75] The capacitances (C), leakage currents (J), and thickness (d) data for $\mathbf{A_x}$ and $\mathbf{B_x}$ v-SANDs are summarized in Table 2.

2. Semiconductor Thin-Film Morphology. 2.1. Pentacene Microstructure As a Function of v-SAND Growth Parameters. Thin-film microstructures, morphologies, and molecular orientations of the semiconductors were studied by $\theta-2\theta$ X-ray diffraction (XRD) and AFM. Thin-film XRD is important for evaluation of the out-of-plane ordering of vapor-deposited small-molecule organic thin films. Often the ordering correlates with carrier mobility, which is generally accepted to be confined within the first few nanometers of the semiconductor at the semiconductor−dielectric interface.[76,77] Since direct characterization of the microstructure at the buried dielectric−semiconductor interface is not possible with conventional techniques, the semiconductor surface and crystallinity across the entire thin film is reasonably[78] assumed to resemble the basic microstructure at the interface. Positions of the 2θ reflections provide lattice plane Bragg d-spacings, while the presence of multiple reflections from the same Bragg family indicates long-range order. AFM images and XRD spectra show that increasing the **F1** and **F2** film thicknesses in the $\mathbf{A_x}$ type of microstructure does not perceptibly affect the pentacene growth behavior.

The pentacene XRD spectra are next compared for films grown on uncapped (Supporting Information Figure S3A) and capped (Supporting Information Figure S3B) v-SANDs. The diffraction data reveal that pentacene films deposited on both uncapped and capped dielectrics are highly crystalline, each having d-spacings of 15.4 Å observed up to the third order on both **F1** and **F2** uncapped films, and up to third and fourth order on **F1-cap** and **F2-cap**, respectively. This particular d-spacing corresponds to the pentacene "thin-film" phase[79,80] and is observed independent of the dielectric film surface (capped vs uncapped films). In the case of uncapped **Fn** films, sulfonic or carboxylic acidic end groups terminate the surface, whereas the surfaces of the **Fn-cap** films are terminated by SiO_x silanol groups. Tapping mode AFM images of pentacene films grown on uncapped v-SANDs (insets of Supporting Information Figure S3A) reveal significantly smaller grains sizes (<0.5 μm) compared to grain sizes of 1−2 μm, which grow on the capped films (Supporting Information Figure S4). Note that no field effect is observed for OFETs using the **Fn** films without the SiO_x **cap** layer (see more below), which is direct evidence that hybrid organic−inorganic gate dielectrics perform differently in OFETs than do the individual components.[81] Thus, the enhanced OFET response properties (discussed below) reflect summing of the properties of the high-permittivity π-conjugated molecular component and the low-leakage SiO_x component. Furthermore, the microstructures of pentacene films deposited on **1**- versus **2**-based v-SANDs are slightly different, where the greater number and intensity of the Bragg reflection peaks on **F1-cap** indicate enhanced crystallinity and long-range order compared to films deposited on **F2-cap**. Additionally, AFM images also reveal *slightly* larger pentacene film texture and grain sizes on **F1-cap** than on **F2-cap**.

2.2. n-Type Semiconductor Microstructure As a Function of v-SAND Growth Parameters. The n-type semiconductors **DFHCO−4TCO** and **TIFDMT** were vapor-deposited directly on v-SANDs having the $\mathbf{A_x}$ microstructure, and the low-voltage OFET performance characteristics were evaluated. Previously, electron transport in **DFHCO-4TCO** and **TIFDMT** was demonstrated, even when the OFETs were operated under ambient conditions.[2,82] Here we investigate n-type transport in these semiconductors under high-vacuum and ambient conditions using v-SANDs as the gate dielectric in place of a thick (300 nm) SiO_2 gate dielectric. XRD data for **DFHCO-4TCO** and **TIFDMT** thin films vapor-deposited on various v-SAND substrates were collected to investigate the out-of-plane ordering. In addition to lattice plane d-spacings, Laue oscillations around the first- and second-order diffraction peaks indicate extremely uniform **DFHCO-4TCO** layer spacings (Figure 5A−C).[69,76] An extensive analysis comparing XRD data for optimized films of **DFHCO-4TCO** grown on SiO_2 has already been reported, and in that study Laue oscillations were not observed.[83]

Thus, v-SAND substrates induce more ordered crystallites in **DFHCO-4TCO**, as evidenced by the Laue oscillations from which the semiconductor film thickness is calculated to be ~30 nm (as deposited). Additionally, the d-spacing is ~30 Å, in agreement with the previously reported[83] value for films on 300 nm thermally grown SiO_2 as the substrate.

Interestingly, greater long-range order and crystallinity of **DFHCO-4TCO** is observed on uncapped v-SAND substrates compared to capped v-SANDs, as evidenced by more intense Laue oscillations[68] and higher-order Bragg reflections.[76] This

(73) Houili, H.; Picon, J. D.; Zuppiroli, L. *J. Appl. Phys.* **2006**, *100*, 023702.
(74) Sihvola, A. *Electromagnetic Mixing Formulas and Applications*; IEE Publishing: London, 1999; Vol. 47.
(75) Ashwell, G. J.; Robinson, B. H.; Mukhtar, A. A.; Locatelli, D.; Quici, S.; Roberto, D. *J. Mater. Chem.* **2005**, *15*, 4203.
(76) Jones, B. A.; Facchetti, A.; Wasielewski, M. R.; Marks, T. J. *Adv. Funct. Mater.* **2008**, *18*, 1329.
(77) Jung, J.; Sun, J.; Lee, T.; Sarjeant, A.; Katz, H. E. *Chem. Mater.* **2009**, *21*, 94.
(78) Lu, G.; Usta, H.; Risko, C.; Wang, L.; Facchetti, A.; Ratner, M. A. *J. Am. Chem. Soc.* **2008**, *130*, 7670.
(79) Yang, H.; Shin, T. J.; Ling, M.-M.; Cho, K.; Ryu, C. Y.; Bao, Z. *J. Am. Chem. Soc.* **2005**, *127*, 11542.
(80) Kim, C.; Facchetti, A.; Marks, T. J. *Adv. Mater.* **2007**, *19*, 2561.
(81) Samokhvalov, A.; Gurney, R. W.; Lahav, M.; Naaman, R. *J. Phys. Chem. B* **2002**, *106*, 9070.
(82) Usta, H.; Facchetti, A.; Marks, T. J. *J. Am. Chem. Soc.* **2008**, *130*, 8580.
(83) Yoon, M.-H.; DiBenedetto, S. A.; Russell, M. T.; Facchetti, A.; Marks, T. J. *Chem. Mater.* **2007**, *19*, 4864.

suggests that the organic functionalities exposed at the surface, possibly the sulfonic or carboxylic acid end groups (or others, depending on molecular alignment on the surface), are more favorable for wetting, nucleation, and ultimately **DFHCO-4TCO** film growth. However, similar to pentacene, uncapped v-SAND based OFETs do not exhibit field-effect response, despite the favorable texturing and crystallinity observed by XRD characterization. This observation is most likely attributable to the large current leakage, or to electrical shorts, through the uncapped films. Furthermore, in a trend opposite to that of pentacene, **DFHCO-4TCO** films are almost completely amorphous on **F2-cap** substrates as evidenced by the low intensity and small number of Bragg diffraction peaks in conjunction with weak Laue oscillation intensities (blue line, Figure 5B), compared to films of **DFHCO-4TCO** grown on **F1-cap** substrates.

Previously, **TIFDMT** was reported to form highly crystalline films (fourth-order Bragg reflections observed) from the solution phase on OTS-treated 300 nm SiO_2 surfaces, with a dominant Bragg reflection at $2\theta = 3.46°$ (d-spacing of 25.6 Å).[82] However, the present vapor-deposited **TIFDMT** films on v-SANDs (Figure 5, parts C and D) exhibit two dominant Bragg reflections at $2\theta = 2.8°$ (d-spacing = 31.5 Å) and $2\theta = 3.45°$ (d-spacing = 25.6 Å), indicating that two dominant phases/orientations are present. Interestingly, the relative intensity of the two reflections is sensitive to the chemical structure of the underlying v-SAND molecule. The intensities of the two reflections on both **F2** and **F2-cap** substrates are nearly identical; however, for **F1** the intensity of the peak at 3.45° is larger and decreases after capping, whereas for **F1-cap** the reflection at 2.8° is more intense. The difference in the **TIFDMT** microstructure on v-SANDs versus that on SiO_2/OTS (previously reported[82]) likely results from surface energy differences,[53] since, unlike the prior **TIFDMT** study, the v-SAND surfaces were not functionalized with a hydrophobic surface treatment prior to semiconductor deposition.

3. OFET Characteristics. OFETs with top-contact/bottom gate device structures were fabricated by vacuum deposition of the semiconductor film directly onto the v-SAND gate dielectrics. The OFET performance using v-SANDs in the $\mathbf{A_x}$ and $\mathbf{B_x}$ microstructural arrangements is presented here. Additionally, an expanded set of organic semiconductors was investigated to test the compatibility of v-SANDs with air-stable, n-type organic semiconductors. Vapor-phase depositions of the semiconductors onto the **Fn-cap** dielectrics were carried out under high vacuum (1×10^{-6} Torr) with the substrates maintained at previously optimized temperatures of 25 (pentacene), 70 (**DFHCO-4TCO**), or 120 °C (**TIFDMT**) during film growth. Gold contacts were patterned by thermal evaporation using shadow masks. OFET electrical properties were evaluated under ambient and high-vacuum conditions and under positive or negative gate biases depending on the semiconductor major charge carrier.

First, in Supporting Information Figure S5 we compare the pentacene OFET characteristics using v-SAND gate dielectrics with either ~3 or ~6 nm of **cap** (with a constant molecular layer thickness of ~3 nm). The MIS leakage current for a **F1-cap** gate dielectric with a 3 nm SiO_x **cap** layer is $\sim 10^{-2}$ A/cm^2 at 2.0 V (Figure 4E, black line). This large leakage current parallels degradation in OFET performance, where the output curves for increasing gate voltages do not all intersect at 0.0 V, as shown in Supporting Information Figure S5B. Additionally, the pentacene OFETs have slightly lower mobilities (1.1 cm^2/(V s)), and I_{on}/I_{off} current ratios (10^4) than OFETs fabricated with gate dielectrics having a 6 nm SiO_x **cap** layer. For **F1-cap** films with 6 nm of SiO_x **cap**, the leakage current drops by 3 orders of magnitude to $\sim 10^{-6}$ A/cm^2 at 2.0 V (Figure 4D, black line), and improvements in both the gate leakage current during OFET operation (Supporting Information Figure S5C) and performance metrics ($\mu = 1.9$ cm^2/(V s) and $I_{on}/I_{off} = 10^5$) are observed.

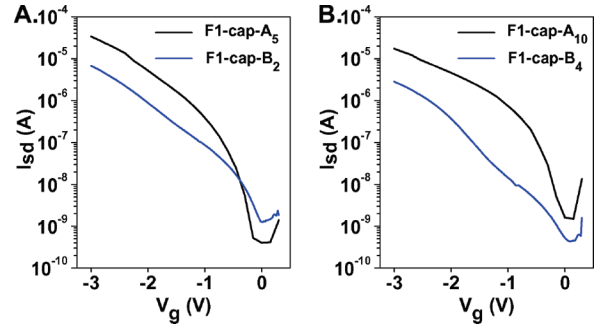

Figure 6. Pentacene FET transfer plots ($V_{sd} = 3.0$ V) comparing the effects of the two different v-SAND microstructures, $\mathbf{A_x}$ vs $\mathbf{B_x}$, on device performance, for thinner $\mathbf{A_5}$ and $\mathbf{B_2}$ microstructures (A) compared to thicker $\mathbf{A_{10}}$ and $\mathbf{B_4}$ (B) v-SAND gate dielectrics.

After optimizing the cap thickness, the trends in pentacene OFET response across the $\mathbf{A_x}$ and $\mathbf{B_x}$ v-SAND series of **F1-** and **F2-cap** gate dielectrics was investigated. For the thicker molecular layers $\mathbf{A_5}$ (Figure 6A) and $\mathbf{A_{10}}$ (Figure 6B), the OFET operating voltage was increased from 2.0 to 3.0 V in order to maintain the same charge accumulation density (n_T) in the pentacene channel as in the thinner $\mathbf{A_3}$ v-SAND samples. The OFET transfer plots using **F1-cap** or **F2-cap** as the gate dielectric remain very similar as the molecular layer thickness is increased.

Hence, the mobilities of 2 and 3 cm^2/V for **F1-cap** and **F2-cap**, respectively, and the threshold voltages (1.1 V) for both **F1-cap** and **F2-cap** remain constant with v-SAND thickness for each $\mathbf{A_x}$ gate dielectric. Furthermore, the output plots of pentacene $\mathbf{A_x}$ **F1-cap** (Figure 7, parts B and E) and $\mathbf{A_x}$ **F2-cap** (Figure 7, parts C and F) based OFETs remain very similar as the dielectric thickness is increased.

In contrast to the $\mathbf{A_x}$ results, the output plots for the $\mathbf{B_x}$ microstructural arrangement differ significantly as the number of organic−inorganic layers is increased. The $\mathbf{B_x}$-based OFET output plots in Figure 7, parts A and D, show that the gate leakage increases with increasing dielectric thickness. This indicates that pentacene OFET performance is sensitive to the arrangement details of the organic and inorganic layers in the v-SAND stack.[65] The largest pentacene mobilities are observed with **F2-cap** dielectrics in the $\mathbf{A_x}$ type of microstructure, and the smallest mobilities are measured on **F1-cap** dielectrics in the $\mathbf{B_x}$ type of microstructure. A summary of pentacene OFET performance parameters is compiled in Table 3.

Since the $\mathbf{A_x}$ v-SAND microstructure is more effective in enhancing OFET performance, OFETs with the n-type semiconductors **DFHCO-4TCO** and **TIFDMT** were investigated using the $\mathbf{A_3}$ type of **F1-** or **F2-cap** as the gate dielectric. Transfer plots of **DFHCO-4TCO** OFETs under vacuum and under ambient conditions are shown in Figure 8, parts A and B, respectively. The **DFHCO-4TCO** electron mobility is ~0.05 cm^2/(V s) under vacuum, and ~0.01 cm^2/(V s) under ambient, for all of the v-SANDs investigated here as gate dielectrics. These mobilities agree well with those reported previously under

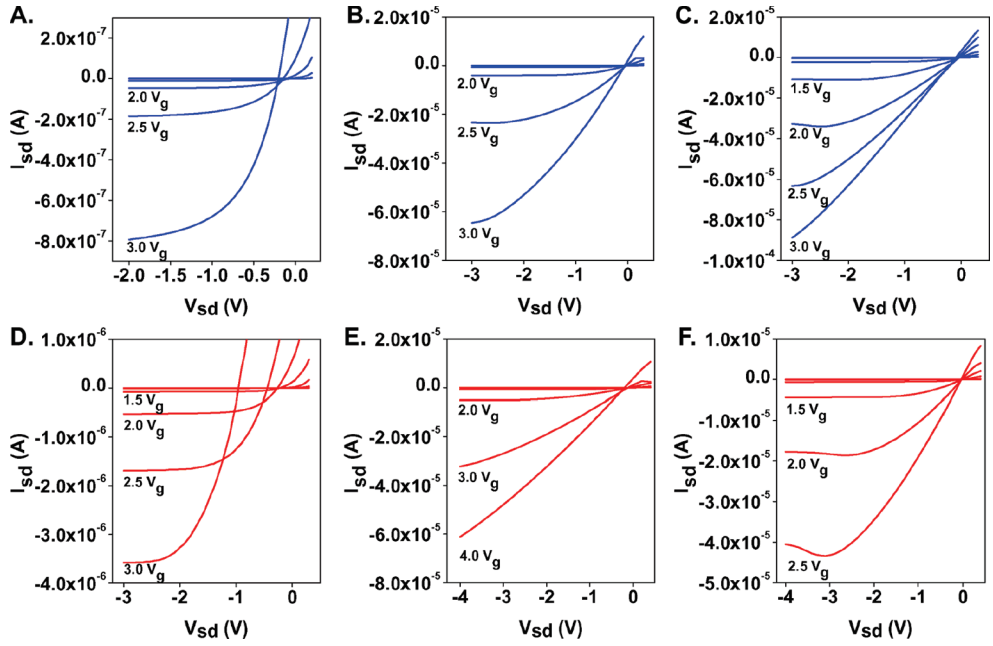

Figure 7. Comparison of pentacene OFET output characteristics using **F1-cap** v-SANDs in the $\mathbf{B}_x$ microstructure (A and D) and **F1-cap** (B and E), or **F2-cap** (C and F) v-SANDs in the $\mathbf{A}_x$ microstructure. The molecular layer thicknesses are ~3 nm for the data in panels A−C and ~10 nm for the data in panels D−F.

Table 3. **F1-cap** and **F2-cap** (d_{tot}), **F1** and **F2** (d_{uncap}) v-SAND, and SiO_x **cap** ($d_{tot} - d_{uncap} = d_{cap}$) Film Thicknesses Measured by XRR[a]

sample	C_{tot} (nF/cm^2)	k_{molec}	μ_h (cm^2/(V s))/V_g (V)	I_{on}/I_{off}	V_T (V)	n_T (cm^{-2})
F1-cap						
A_3	375	11.0	1.9/2.0	10^5	1.1	4.7×10^{19}
A_5	237	9.5	2.0/3.0	10^5	1.5	4.4×10^{19}
A_{10}	165	3.6	2.1/3.0	10^3	1.1	4.1×10^{19}
F2-cap						
A_3	392	9.4	2.6/2.0	10^4	0.80	4.9×10^{19}
A_5	265	12.3	3.3/3.0	10^4	1.1	4.9×10^{19}
A_{10}	185	12.0	3.6/3.0	10^4	1.2	4.6×10^{19}
F1-cap						
B_1	425	4.0	1.1/2.0	10^4	0.67	5.3×10^{19}
B_2	307	5.9	0.74/3.0	10^4	1.6	5.7×10^{19}
B_3	227	8.4	0.29/3.0	10^4	1.12	4.3×10^{19}
B_4	187	7.5	0.45/3.0	10^4	1.5	3.5×10^{19}

[a] MIS measured capacitances (C_{tot}) and estimated dielectric permittivities (k) of v-SANDs. Pentacene OFET characteristics: μ_h, operating voltage (V_g), current on/off ratio (I_{on}/I_{off}), threshold voltage (V_T), and charge accumulation density at the interface (n_T). Total thicknesses include 1.5 nm native SiO_2 on the n^+-Si gate.

ambient conditions on thick SiO_2 gate dielectrics,[2] demonstrating that **DFHCO-4TCO** films on unconventional gate dielectrics have the same electron transport efficiency and ambient stability at much lower operating voltages. The **DFHCO-4TCO** OFET characteristics on the different v-SAND gate dielectrics can be explained by the semiconductor crystallinity, where **DFHCO-4TCO** films deposited on **F2-cap** have the same d-spacing as films grown on SiO_2 (Table 4). For OFETs using **F2-cap**, the I_{on}/I_{off} ratio is the largest (10^7) under vacuum. However, all films exhibit smaller I_{on}/I_{off} ratios under ambient conditions. Additionally, the threshold voltages of **DFHCO-4TCO** FETs shift to smaller values in ambient (Table 4). Typically, threshold voltage shifts indicate the presence of traps either in the dielectric or at the semiconductor−dielectric interface.[76,84]

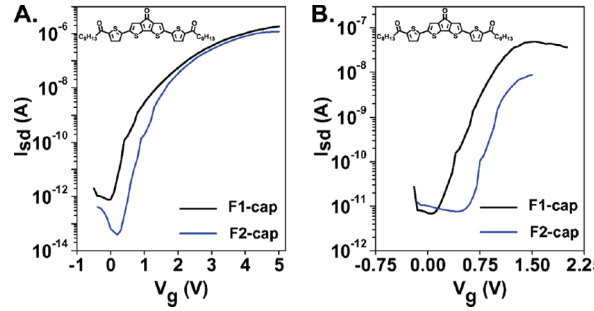

Figure 8. OFET transfer plots for **DFHCO-4TCO** on v-SANDs: (A) under high vacuum, where the black line indicates **F1-cap** ($V_{sd} = 3.0$ V), and the blue line is indicates **F2-cap** ($V_{sd} = 3.0$ V) as the gate dielectric, and (B) in ambient, where the black line indicates **F1-cap** ($V_{sd} = 2.0$ V), and the blue line is indicates **F2-cap** ($V_{sd} = 1.5$ V) as the gate dielectric.

Under high-vacuum conditions, the **DFHCO-4TCO** $I-V_{SD}$ scans for each V_G intersect at a single point (Figure 9A). However, under ambient conditions (Figure 8B) the output plots exhibit poor field-effect performance, which is likely due to trapping and increased gate leakage current at the dielectric−semiconductor interface.[85−87]

The v-SAND-based **TIFDMT** OFETs exhibit similar transfer and output characteristics to those of the **DFHCO-4TCO** OFETs, except that the v-SAND gated OFETs exhibit reduced performance compared to OFETs previously reported on thick OTS-treated SiO_2.[82] This is most likely attributable to the two dominant crystalline phases observed in the present XRD spectra. Films composed of multiple phases or different growth

(84) Wang, S. D.; Minari, T.; Miyadera, T.; Aoyagi, Y.; Tsukagoshi, K. *Appl. Phys. Lett.* **2008**, *92*, 063305.
(85) Jones, B. A.; Facchetti, A.; Wasielewski, M. R.; Marks, T. J. *J. Am. Chem. Soc.* **2007**, *129*, 15259.
(86) Chabinyc, M. L.; Endicott, F.; Vogt, B. D.; DeLongchamp, D. M.; Lin, E. K.; Wu, Y.; Liu, P.; Ong, B. S. *Appl. Phys. Lett.* **2006**, *88*, 113514.
(87) Mathijssen, S. G. J.; Kemerink, M.; Sharma, A.; Colle, M.; Bobbert, P. A.; Janssen, R. A. J.; de Leeuw, D. M. *Adv. Mater.* **2008**, *20*, 975.

Table 4. **DFHCO-4TCO** OFET Characteristics with v-SAND Gate Dielectrics[a]

dielectric	d_{tot} (nm)	C_{tot} (nF/cm^2)	Bragg d-spacing	μ_{vac} (μ_{air}) (cm^2/(V s))	$I_{on}/I_{off,vac}$ ($I_{on}/I_{off,air}$)	$V_{T,vac}$ ($V_{T,air}$) (V)	ΔV_T
SiO_2/OTS	300	12.0	30.2	0.08 (0.01)	10^7	9	
F2-cap	15.0	312	30.1	0.04 (0.01)	10^7 (10^3)	−1.5 (−0.8)	0.76
F1-cap	24.4	300	28.6	0.05 (0.02)	10^6 (10^3)	−1.5 (−0.6)	0.92

[a] XRR measured thicknesses (d_{tot}) and MIS measured capacitances (C_{tot}) of v-SANDs. OFET characteristics under vacuum (vac) and under ambient (air) conditions: mobility (μ_e), current on/off ratio (I_{on}/I_{off}), threshold voltage (V_T), and threshold voltage shift ($\Delta V_T = V_{T,vac} - V_{T,air}$).

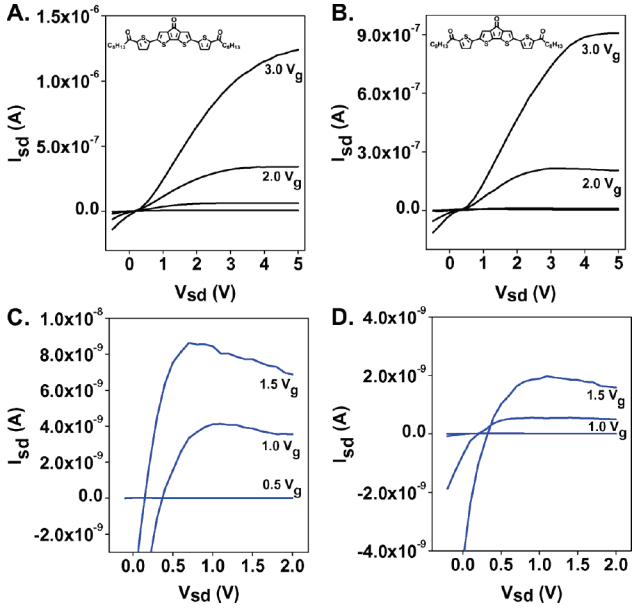

Figure 9. **DFHCO-4TCO** OFET output plots on v-SANDs under vacuum (black curves, in panels A and B) and in ambient (blue curves, in panels C and D). OFETs were fabricated with the indicated gate dielectrics: **F1-cap** (A and C)) and **F2-cap** (B and D).

orientations of the same phase are not ideal for high-mobility OFETs since dislocations of the grain boundaries limit charge transfer between the source and drain electrodes.[88−90] For **TIFDMT**, optimum performance is observed for OFETs fabricated with **F1-cap** as the gate dielectric, where the mobilities approach 10^{-2} cm^2/(V s) and the I_{on}/I_{off} ratios are 10^4 under both vacuum and ambient conditions. Similar to **DFHCO-4TCO**, the threshold voltage shifts to smaller values for devices operated under ambient conditions. Summaries of the OFET performance characteristics for **DFHCO-4TCO** and **TIFDMT** are compiled in Tables 4 and 5, respectively.

4. Consequences of Film Growth Details for Electrical Properties. The orientation of film component molecules with respect to the surface is crucial for optimum dielectric response.[91] For practical applications, the largest polarization P, which is a sum of the dipole vectors ($P = \langle\mu\rangle N$, also see Figure 10 for dipole illustration), should be perpendicular to the substrate and parallel to the direction of the applied field (E) and molecular orientation (called linear growth).[92−97] Nonlinear growth is observed when the dipoles are aligned antiparallel to each other in dipole−dipole aggregation (Figure 10C)[95] and/or when the π-conjugated molecular backbone is oriented with a large tilt angle with respect to the surface normal (Figure 10B).[98,99]

An informative test of dipolar regularity in thin films is the second-harmonic generation (SHG) response as a function of film thickness.[93,100−102] For molecular structures similar to **1** and **2**, it has been demonstrated that polar alignment of the dipoles results in large SHG responses,[19] where linear orientation of the dipoles is promoted by strong self-organizing pyridine−HOOC hydrogen-bonding interactions.[94,103−105] As such, the film growth characteristics of molecules **1** and **2** have been extensively investigated (Supporting Information Figure S6),[99] and it was found that molecule **1** grows nonlinearly for film thicknesses greater than ~3 nm, resulting from either large tilt angle hydrogen-bonding interactions (Figure 10B) or dipolar aggregation (Figure 10C), whereas **2** grows with linear head-to-tail ordering (Supporting Information Figure S6B).[99]

Thus, correlations between v-SAND component molecular structure and OFET electrical properties is not straightforward since **1** and **2** engage in different hydrogen-bonding interactions (sulfonic vs carboxylic) and thin-film dipolar ordering.[106] For the nonalternating $\mathbf{A_x}$ arrangement of organic and inorganic dielectric components, the permittivity of **F1** decreases with increasing molecular layer thickness and is most likely a direct result of propagation of the nonlinear dipolar order as the **F1** thickness increases. In contrast, the permittivities of **F2** ($\mathbf{A_5}$−$\mathbf{A_{10}}$) remain almost invariant (Table 2) after a slight enhancement from the thin $\mathbf{A_3}$ sample. This is in good agreement with the enhanced SHG response as the **F2** thickness increases (Supporting Information Figure S6B). For the $\mathbf{B_x}$ microstructural arrangement, the permittivities actually increase as the total

(88) Kim, C. S.; Jo, S. J.; Lee, S. W.; Kim, W. J.; Baik, H. K.; Lee, S. J. *Adv. Funct. Mater.* **2007**, *17*, 958.
(89) Facchetti, A.; Letizia, J. A.; Yoon, M.-H.; Mushrush, M.; Katz, H. E.; Marks, T. J. *Chem. Mater.* **2004**, *16*, 4715.
(90) Letizia, J. A.; Salata, M. R.; Tribout, C. M.; Facchetti, A.; Ratner, M. A.; Marks, T. J. *J. Am. Chem. Soc.* **2008**, *130*, 9679.
(91) Liao, Y.; Battacharjee, S.; Firestone, K. A.; Eichinger, B. E.; Paranji, R.; Anderson, C. A.; Robinson, B. H.; Reid, P.; Dalton, L. R. *J. Am. Chem. Soc.* **2006**, *128*, 6847.
(92) Kumar, U.; Frechet, J. M. J.; Kato, T.; Ukie, S.; Timura, K. *Angew. Chem., Int. Ed.* **1992**, *31*, 1531.
(93) Ashwell, G. J.; Jackson, P. D.; Crosslnad, W. A. *Nature* **1994**, *368*, 438.
(94) Rashid, A. N.; Erny, C.; Gunter, P. *Adv. Mater.* **2003**, *15*, 2024.
(95) Kahn, R. U. A.; Kwon, O.-P.; Tapponnier, A.; Rashid, A. N.; Gunter, P. *Adv. Funct. Mater.* **2006**, *16*, 180.
(96) Philip, B.; Sreekumar, K. *Colloid Polym. Sci.* **2003**, *281*, 385.
(97) Bhattacharya, M.; Yoon, W.-J.; Berger, P. R.; Timmons, R. B. *Adv. Mater.* **2008**, *20*, 2383.
(98) de Matos Gomes, E.; Rodrigues, V. H.; Costa, M. M. R.; Belsley, M. S.; Cardoso, P. J. M.; Goncalves, C. F.; Procenca, F. *J. Solid State Chem.* **2006**, *179*, 2521.
(99) Frattarelli, D.; Schiavo, M.; Facchetti, A.; Ratner, M. A.; Marks, T. J. *J. Am. Chem. Soc.*, submitted for publication, **2009**.
(100) Garg, A.; Davis, R. M.; Durak, C.; Heflin, J. R.; Gibson, H. W. *J. Appl. Phys.* **2008**, *104*, 053116.
(101) Zhang, W.-K.; Wang, H.-F.; Zheng, D.-S. *Phys. Chem. Chem. Phys.* **2006**, *8*, 4041.
(102) Kang, H.; Evmenenko, G.; Dutta, P.; Clays, K.; Song, K.; Marks, T. J. *J. Am. Chem. Soc.* **2006**, *128*, 6194.
(103) Facchetti, A.; Marks, T. J. *Nat. Mater.* **2004**, *3*, 910.
(104) Rochefort, A.; Bayard, E.; Hadj-Messaoud, S. *Adv. Mater.* **2007**, *19*, 1992–1995.
(105) Shirman, T.; Freeman, D.; Posner, Y. D.; Feldman, I.; Facchetti, A.; van der Boom, M. E. *J. Am. Chem. Soc.* **2008**, *130*, 8162.
(106) Datta, A.; Pati, S. K. *J. Mol. Struct. (THEOCHEM)* **2005**, *756*, 97.

Table 5. **TIFDMT** OFET Characteristics with v-SAND Gate Dielectrics[a]

dielectric	d_{tot} (nm)	C_{tot} (nF/cm^2)	Bragg d-spacing	μ_{vac} (μ_{air}) (cm^2/(V s))	$I_{on}/I_{off,vac}$ ($I_{on}/I_{off,air}$)	$V_{T,vac}$ ($V_{T,air}$) (V)	ΔV_T
SiO_2/OTS	300	12.0	25.6	(0.1)	(10^7)	(5.0)	
F2-cap	15.0	312	25.6	3×10^{-3} (1×10^{-3})	10^3 (10^1)	−1.0 (−0.7)	0.49
F1-cap	16.1	260	25.6	6×10^{-3} (7×10^{-3})	10^4 (10^4)	−1.2 (−0.7)	0.54

[a] XRR measured thicknesses (d_{tot}) and MIS measured capacitances (C_{tot}) of v-SANDs. OFET characteristics under vacuum (vac) and under ambient (air) conditions: mobility (μ_e), current on/off ratio (I_{on}/I_{off}), threshold voltage (V_T), and threshold voltage shift ($\Delta V_T = V_{T,vac} - V_{T,air}$).

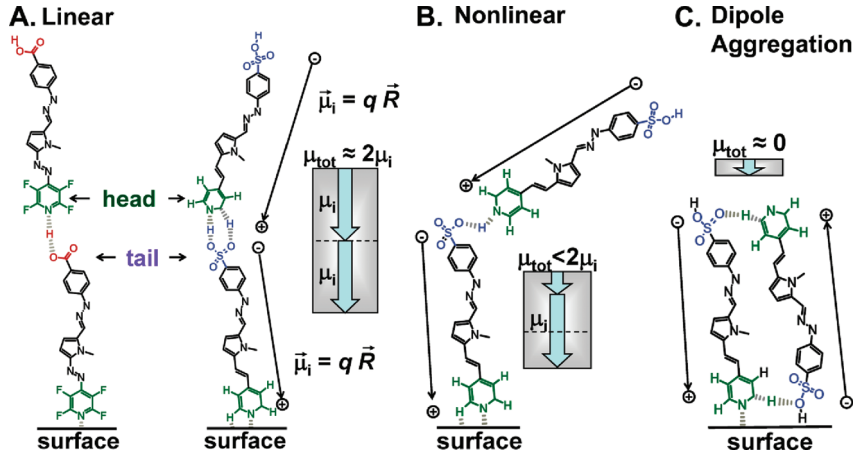

Figure 10. Cartoons of possible head-to-tail hydrogen-bonding interactions governing the molecular orientation in (A) linear, (B) nonlinear, and (C) aggregated dipolar orientations. The chromophores are simplified as dipoles, and vector addition results in different bulk polarizations, represented as the gray boxes.

alternating microstructure thickness is increased.[107] In conjunction with the XRR data shown in Figure 4D−F, this is strong evidence for linear dipolar order and enhanced polarization (P). Thus, it seems plausible that alternating SiO_x **cap** interfacial layers with **F1** layers effectively disrupts the nonlinear growth of molecule **1** and the thin capping layers regenerate hydrophilic surface hydrogen-bonding sites, which enable linear growth of the next molecular layer.[10]

Further evidence that the molecules are better aligned in the $\mathbf{B_x}$ microstructure comes from the larger capacitances of the $\mathbf{B_x}$ **F1-cap** films compared to $\mathbf{A_x}$ **F1-cap**, where the $\mathbf{A_{10}}$ sample has a lower capacitance than both the thickest alternating film ($\mathbf{B_4}$) and the calculated parallel plate capacitance (Figure 4A). Furthermore, the $\mathbf{B_x}$-gated pentacene OFET performance is reduced from that of the $\mathbf{A_x}$-gated pentacene OFETs (Table 3). As the $\mathbf{B_x}$ film thickness increases, μ_h drops from 1.0 to 0.4 cm^2/(V s), the threshold voltage increases from 0.7 to 1.5 V, and the charge accumulation (n_T)[108] decreases as the total $\mathbf{B_x}$ film thickness is increased. This is most likely due to the large leakage currents through the $\mathbf{B_x}$ films (Figure 5E).[109]

Given that all v-SAND structures have the SiO_x **cap** in contact with pentacene, and that the pentacene grain texturing is similar (AFM images, Supporting Information Figure S4), the difference between the present observed pentacene mobilities cannot be explained entirely on the basis of conventional semiconductor−dielectric interface[51,108,110] and pentacene film morphology[80,111−113] arguments. Note that several groups have explored correlations between pentacene grain size and charge mobility,[114−117] with most reporting increased mobility with increased pentacene grain size,[88,118] although many aspects remain unresolved.[1,108] For example, one report claims that low dielectric permittivity gate dielectrics are ideal for OFETs since large-permittivity dielectrics induce organic semiconductor charge carrier localization via dielectric polarization enhanced strong dipole moments. However, in the same study,[119] the authors claim that a multilayer structure consisting of a high-permittivity layer in combination with a low-permittivity layer deposited on top should maximize capacitance and minimize interface trapping in top-contact OFETs. Indeed, pentacene OFET performance and grain size are increased when v-SANDs (which are fabricated in the multilayered $\mathbf{A_x}$ microstructure) are used as the gate dielectric in place of conventional SiO_2 gate dielectrics.

This work also shows that pentacene hole mobilities are larger in OFETs fabricated with the higher-capacitance **F2-cap** gate dielectrics; however, the opposite trend is observed for n-type OFETs, where slightly larger electron mobilities are measured in devices fabricated with the lower-capacitance **F1-cap** $\mathbf{A_x}$ microstructure. Interestingly, similar results have been observed for p- and n-type semiconductors on SiO_2 gate dielectrics having

(107) Richards, T.; Bird, M.; Sirringhaus, H. *J. Chem. Phys.* **2008**, *128*, 234905.
(108) Yoon, M.-H.; Kim, C.; Facchetti, A.; Marks, T. J. *J. Am. Chem. Soc.* **2006**, *128*, 12851.
(109) Mottaghi, M.; Horowitz, G. *Org. Electron.* **2006**, *7*, 528.
(110) Lin, Y.-Y.; Gundlach, D. J.; Nelson, S. F.; Jackson, T. N. *IEEE Electron. Device* **1997**, *44*, 1325.
(111) Park, Y. D.; Lim, J. A.; Lee, H. S.; Cho, K. *Mater. Today* **2007**, *10*, 46.
(112) Yokoyama, T.; Park, C. B.; Nagashio, K.; Kita, K.; Toriumi, A. *Appl. Phys. Exp.* **2008**, *1*, 041801.
(113) Lee, H. S.; Kim, D. H.; Cho, J. H.; Hwang, M.; Jang, Y.; Cho, K. *J. Am. Chem. Soc.* **2008**, *130*, 10556.
(114) Orgiu, E.; Taki, M.; Fraboni, B.; Looci, S.; Bonfiglio, A. *Appl. Phys. Lett.* **2008**, *93*, 043311.
(115) Lee, H. S.; Kim, D. H.; Cho, J. H.; Park, Y. D.; Kim, J. S.; Cho, K. *Adv. Funct. Mater.* **2006**, *16*, 1859.
(116) Locklin, J.; Roberts, M.; Mannsfeld, S.; Zhenan, B. *Polym. Rev.* **2006**, *46*, 79.
(117) deLongchamp, D. M.; Sambasivan, S.; Fischer, D. A.; Lin, E. K.; Chang, P.; Murphy, A. R.; Frechet, J. M. J.; Vivek, S. *Adv. Mater.* **2005**, *17*, 2340.
(118) Kim, C.; Facchetti, A.; Marks, T. J. *Adv. Mater.* **2007**, *19*, 2561.
(119) Veres, J.; Ogier, S. D.; Leeming, S. W.; Cupertino, D. C.; Khaffaf, S. M. *Adv. Funct. Mater.* **2003**, *13*, 199.

fluorocarbon (polar) and alkane chain (nonpolar) SAM surface treatments, where the fluorocarbon SAM supports larger hole mobilities but reduced electron mobilities.[55,120] However, the differences in n-type performance observed in the present study are very small, suggesting that electron transport in n-type organic semiconductors is much more sensitive to the dielectric−semiconductor interface than hole transport in p-type organic semiconductors, as has been demonstrated before.[121,122] Also, the presence of threshold voltage shifts and degraded output curves for devices operated in ambient further supports the contention that the interface dominates n-type transport in v-SAND gated OFETs.

Nonetheless, a direct correlation between large pentacene hole mobilities and high-capacitance v-SAND gate dielectrics is observed here, and likewise, a slight enhancement of n-type performance can be correlated with low-capacitance v-SANDs. It is also likely that different molecular or polymeric capping materials with hydrophobic organic functionalities will increase the n-type OFET performance above that observed here.[58,87,123] Furthermore, the ease of the solventless fabrication demonstrated here is useful for future flexible electronics since v-SANDs are deposited from the vapor phase and at room temperature,[97,124] which are desirable attributes for compatibility with flexible substrates in bottom gate, or with organic semiconductors in bottom-contact, OFETs.

Conclusions

OFETs using hybrid v-SAND gate dielectrics and vapor-deposited organic semiconductor layers were fabricated and characterized. v-SAND gate dielectrics undergo self-assembly via molecular precursor hydrogen-bonding interactions during film growth. These gate dielectrics consist of two components, a molecular organic layer and an inorganic capping layer. The structural differences between the alternating ($\mathbf{B}_x$) and nonalternating ($\mathbf{A}_x$) microstructural arrangements of the molecular components have been correlated with MIS and OFET electrical properties. The results presented here show that v-SANDs can be used in place of SiO_2 for low-voltage OFET operation for both n-type and p-type organic semiconductors, with performance metrics that are comparable to, or even surpass, those measured using other SAM or thick SiO_2 gate dielectrics.[23,27,118,125] Additionally, we present strong evidence (XRR and electrical) for v-SAND microstructural changes based on different dipolar hydrogen-bonding interactions, resulting in enhanced polarization of the v-SAND films. However, the alternating bilayer $\mathbf{B}_x$ microstructure (with the largest capacitances) exhibits the poorest OFET performance. Likewise, the present v-SAND/**DFHCO-4TCO** OFETs exhibit similar ambient device performance as previously reported with SiO_2 as the gate dielectric, although at much lower operating voltages; however, **TIFDMT** OFET performance operation is much poorer here than previously reported. These results indicate that other factors such as current leakage and interface/surface properties strongly affect OFET transport, thereby complicating one-to-one correlations of capacitance with OFET mobility. Nonetheless, when the organic and inorganic components are fabricated together in the alternating $\mathbf{A}_x$ microstructure, the combined properties of large polarization and large current tunneling barrier (SiO_x) are fully utilized to yield optimal OFET gate dielectrics.

Acknowledgment. We thank Dr. H. Usta for providing samples of the **TIFDMT** semiconductor and Dr. Guennadi Evmenenko for helpful discussions about XRR spectra analysis. This work was supported by the ONR MURI Program (N00014-02-1-0909). We thank the NSF MRSEC program (DMR-0520513) for support of the characterization facilities at the Materials Research Center of Northwestern University.

Supporting Information Available: Experimental sections including Materials and Methods, Device Fabrication and Electrical Measurements, and Modeling Methods; AFM images and SHG response data for **F1** and **F2**;[99] MIS and OFET electrical data for varying thicknesses of the capping layer; complete ref 30. This material is available free of charge via the Internet at http://pubs.acs.org.

JA902751E

(120) Huang, C.; Katz, H. E.; West, J. E. *Langmuir* **2007**, *23*, 13223.
(121) Chua, L.-L.; Zaumseil, J.; Chang, J.-F.; Ou, E. C.-W.; Ho, P. K.-H.; Sirringhaus, H.; Friend, R. H. *Nature* **2005**, *434*, 194.
(122) Newman, C. R.; Frisbie, D.; da Silva, F. D.; Bredas, J.-L.; Ewbank, P. C.; Mann, K. R. *Chem. Mater.* **2004**, *16*, 4436.
(123) Rajesh, K.; Chandra, M. S.; Hirakawa, S.; Kawamata, J.; Radhakrishnan, T. P. *Langmuir* **2007**, *23*, 8560.
(124) Majewski, L. A.; Schroeder, R.; Grell, M. *J. Phys. D: Appl. Phys.* **2004**, *37*, 21.
(125) Ma, H.; Acton, O.; Ting, G.; Ka, J. W.; Yip, H.-L.; Tucker, N.; Schofield, R.; Jen, A. K.-Y. *Appl. Phys. Lett.* **2008**, *92*, 113303.